THE JOURNAL OF PHYSICAL CHEMISTRY A

Article

pubs.acs.org/JPCA

Reactivity of Liquid and Semisolid Secondary Organic Carbon with Chloride and Nitrate in Atmospheric Aerosols

Bingbing Wang,*[,†] Rachel E. O'Brien,[‡,§] Stephen T. Kelly,[‡] John E. Shilling,[∥] Ryan C. Moffet,[§] Mary K. Gilles,[‡] and Alexander Laskin*[,†]

[†]Environmental Molecular Sciences Laboratory, Pacific Northwest National Laboratory, Richland, Washington 99354 United States

[‡]Chemical Sciences Division, Lawrence Berkeley National Laboratory, Berkeley, California 94720, United States

[§]Department of Chemistry, University of the Pacific, Stockton, California 95211, United States

[∥]Atmospheric Sciences and Global Change Division, Pacific Northwest National Laboratory, Richland, Washington 99354, United States

Supporting Information

ABSTRACT: Constituents of secondary organic carbon (SOC) in atmospheric aerosols are often mixed with inorganic components and compose a significant mass fraction of fine particulate matter in the atmosphere. Interactions between SOC and other condensed-phase species are not well understood. Here, we investigate the reactions of liquid-like and semisolid SOC from ozonolysis of limonene (LSOC) and α-pinene (PSOC) with NaCl using a set of complementary microspectroscopic analyses. These reactions result in chloride depletion in the condensed phase, release of gaseous HCl, and formation of organic salts. The reactions attributed to acid displacement by SOC acidic components are driven by the high volatility of HCl. Similar reactions can take place in SOC/$NaNO_3$ particles. The results show that an increase in SOC mass fraction in the internally mixed SOC/NaCl particles leads to higher chloride depletion. Glass transition temperatures and viscosity of PSOC were estimated for atmospherically relevant conditions. Data show that the reaction extent depends on SOC composition, particle phase state and viscosity, mixing state, temperature, relative humidity (RH), and reaction time. LSOC shows slightly higher potential to deplete chloride than PSOC. Higher particle viscosity at low temperatures and RH can hinder these acid displacement reactions. Formation of organic salts from these overlooked reactions can alter particle physiochemical properties and may affect their reactivity and ability to act as cloud condensation and ice nuclei. The release and potential recycling of HCl and HNO_3 from reacted aerosol particles may have important implications for atmospheric chemistry.

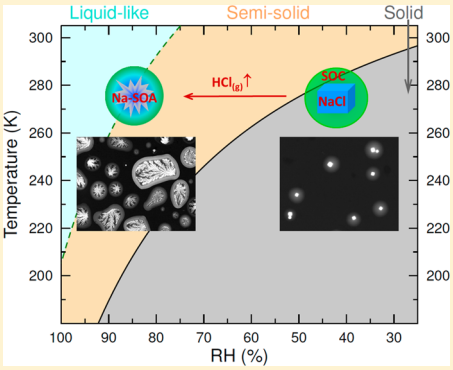

1. INTRODUCTION

Atmospheric aerosol particles play important roles in atmospheric chemistry, global radiation budget, hydrological cycle, climate, and health.[1−4] Particles affect radiation directly by scattering and absorbing radiation and indirectly through aerosol−cloud interactions by acting as cloud condensation and ice nuclei.[5−9] They can also alter atmospheric gas and condensed phase species through various multiphase reactions. SOC originating from oxidation of anthropogenic and biogenic volatile organic compounds represent a significant portion of fine particle mass.[10−12] Recent studies showed that SOC can adopt liquid, semisolid (viscous), and solid phase states depending on the composition and ambient conditions.[13,14] Physical properties, interactions with water vapor, gas-particle partitioning, and reactivity of SOC in aerosol particles may strongly depend on its phase state and viscosity.[6,13−33] Effects of phase states on the SOC reactivity with other atmospheric constituents are poorly understood. To date, few studies have investigated the effects of particle phase on gas-particle uptake of NO_3, O_3, and NH_3.[15,18,21,25,27,34] To our knowledge, there are no studies that examine the reactivity of SOC with condensed-phase species as a function of particle phase states. Here, we investigate the reactivity of SOC with chloride and nitrate and its dependence on SOC phase state and viscosity, particle mixing state, temperature, RH, and reaction time.

The glass transition temperature, T_g, is the transition point between liquid/semisolid and solid states. T_g can be used as a representative temperature below which SOC is in an amorphous solid state and above which SOC adopts a semisolid or liquid state.[18,35−37] For organic particles, various factors can affect T_g including molecular weight of organics, oxidation level (O/C ratio), mixing state, and water content.[6,18] In equilibrium, RH is equal to the water activity (a_w) and determines the water content of particles. Water (T_g of 136 K) can serve as a plasticizer in particles and reduce the T_g of

Special Issue: Mario Molina Festschrift

Received: October 13, 2014
Revised: November 10, 2014
Published: November 11, 2014

   dx.doi.org/10.1021/jp510336q | J. Phys. Chem. A 2015, 119, 4498−4508

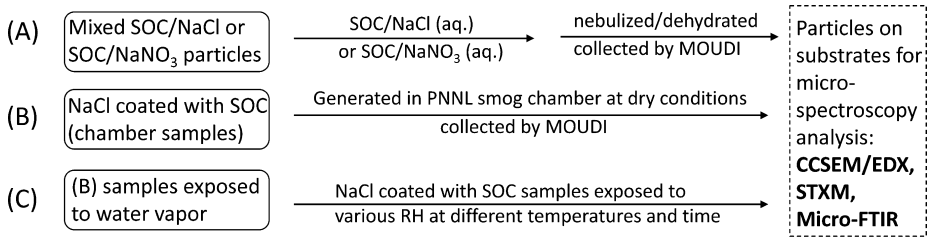

Figure 1. Summary of the investigated particle samples: (A) internally mixed SOC/NaCl particles at 1:1, 4:1, 8:1, and 16:1 mass ratios, and internally mixed SOC/$NaNO_3$ particles at 4:1 mass ratio; (B) SOC-coated NaCl particles generated in PNNL chamber; (C) SOC-coated NaCl particles exposed to various RH (>95%, 80%, and 65%) at 295 and 272 K. Investigated SOC including LSOC and PSOC. See the text for more details.

particles with organic components.[13,38] As such, organic particles with higher water content have lower T_g. Thus, RH is an important factor for determining the physical state of particles. Dynamic viscosity (η) can be used to characterize and distinguish between liquid ($\eta < 10^2$ Pa s), semisolid ($\sim 10^2 - 10^{12}$ Pa s), and solid states ($>10^{12}$ Pa s).[18] η can also be used to estimate the diffusion coefficient of organic species or other species within atmospheric particles.[18]

There is increasing evidence that organic acids can react with inorganic particles through multiphase gas-particle[39−42] and aqueous reactions.[43−49] Recently, we reported that condensed-phase water-soluble organic acids (noted as HA(org) herein) can efficiently react with chloride and nitrate particles resulting in organic salt formation and release of gaseous HCl and HNO_3, a conclusion inferred from both field and laboratory studies.[43−47,50,51] Gaseous HCl or HNO_3 is released from aerosolized internally mixed HA(org)/inorganic particles as a result of acid displacement through similar reaction mechanisms R1 and R2. These reactions are driven by the higher volatility of gas phase HCl and HNO_3 products compared to the volatility of HA(org).[43−47,50,51] Reducing particle water content (decreasing RH) increases HCl and HNO_3 concentrations in aqueous particles. This will partition more HCl and HNO_3 into the gas phase and shift the equilibrium of reactions R1 and R2 to the right. Thus, the kinetics of these reactions can be greatly enhanced when particles undergo dehydration/hydration cycles.

$$NaCl_{(aq)} + HA(org)_{(aq,g)} \leftrightarrow NaA(org)_{(aq,s)} + HCl_{(aq,g)}\uparrow \quad (R1)$$

$$NaNO_{3(aq)} + HA(org)_{(aq,g)} \leftrightarrow NaA(org)_{(aq,s)} + HNO_{3(aq,g)}\uparrow \quad (R2)$$

Here, NaA(org) denotes the corresponding salts of HA(org). HA(org) may originate both from primary emissions and secondary organic formation. To better understand interactions between HA(org) and inorganic components of atmospheric particles, a systematic investigation was conducted on the reactions of SOC with NaCl and $NaNO_3$ using a set of complementary microspectroscopy techniques. The analyses include computer controlled scanning electron microscopy with energy dispersive X-ray analysis (CCSEM/EDX), scanning transmission X-ray microscopy with near edge X-ray absorption fine structure spectroscopy (STXM/NEXAFS), and Fourier transform infrared microspectroscopy (micro-FTIR). These analyses provide comprehensive information on changes in particle morphology, elemental composition, mixing state, and chemical bonding due to the reactions discussed above. T_g and η as a function of temperature and RH for PSOC were estimated to provide further insights into the reaction mechanisms and the controlling factors. The results show a significant effect of particle phase state and viscosity on SOC reactivity and that the reactions are also affected by SOC composition and reaction time.

2. EXPERIMENTAL METHODS

2.1. Sample Preparation. Figure 1 provides a graphic summary of particle samples used in this study and their preparation methods.

First Set of Samples (Figure 1A). Particles were generated from mixed aqueous solutions of secondary organic carbon (SOC) and NaCl (or $NaNO_3$) at different mass ratios. Solutions with a total concentration of 0.2 g/L were used. Limonene SOC (LSOC) and α-pinene SOC (PSOC) were generated by dry ozonolysis of the corresponding precursor in an inflatable Teflon reaction chamber. The chamber was first filled with 400 L air and approximately 1 ppm of O_3 at room temperature and RH < 5%. Then a 10 μL mixture containing 75% (in volume) cyclohexane and 25% of D-limonene or α-pinene was injected in the chamber. Additional details on SOC generation are published elsewhere.[52] After 40 min of reaction time, SOC was collected on aluminum foil substrates, and the SOC was dissolved in deionized water (resistivity ≥18MΩ·cm). $NaNO_3$ (>99%), NaCl (>99%), cyclohexane, D-limonene, and α-pinene (>98%) were obtained from Sigma-Aldrich. Aqueous particles were first nebulized from solutions and then dehydrated by passing through a diffusion dryer. The RH at the end of the dryer was <35% at ~295 K. After the diffusion dryer, the particles were collected onto substrates prearranged on the seventh and eighth stages (cutoff size, D_{50} = 0.56 and 0.32 μm) of a Multi-Orifice Uniform Deposition Impactor (MOUDI; model 110-R, MSP, Inc.). Samples were collected onto grid-supported carbon-filmed grids (Copper 400 mesh grids coated with Carbon Type-B films, Ted Pella, Inc.) for CCSEM/EDX and STXM/NEXAFS analysis, and onto Si_3N_4 windows (100 nm thickness, Silson Ltd.) for micro-FTIR analysis.

The Second Set of Samples (Figure 1B). Particles of NaCl coated with either LSOC or PSOC (thereafter referred as "SOC-coated particles") were generated by condensing SOC onto size selected NaCl seeding particles (~100 nm) from the ozonolysis of corresponding precursor at dry condition (<5%) in continuous flow environmental chamber at Pacific Northwest National Laboratory (PNNL).[53,54] The particles were then collected onto the substrates by MOUDI as described above. The temperature inside the chamber was maintained at 292 and 295 K for LSOC and PSOC generation, respectively. Particle size distributions were measured using Scanning Mobility Particle Sizer (SMPS, TSI 3936) and a Condensation Particle Counter (CPC, TSI 3775).

dx.doi.org/10.1021/jp510336q | J. Phys. Chem. A 2015, 119, 4498−4508

The Third Set of Samples (Figure 1C). NaCl particles coated with SOC were exposed to various RH (>95%, 80%, and 65%) at 295 and 272 K for 8−25 h. The setup for exposure experiments is shown in Supporting Information (SI) Figure S1. Particle samples were exposed to humidified N_2 gas generated by mixing a dry N_2 flow and a water vapor saturated N_2 flow. The RH was adjusted by changing the dry and water vapor saturated N_2 flow rates.[55] Sample temperature was controlled by the water bath. A minimum of three independent samples were analyzed for each particle composition. Over 60 000 individual particles were analyzed by CCSEM/EDX. Except where specifically discussed later, generally particles were dehydrated prior to analysis.

2.2. CCSEM/EDX Analysis and X-ray Mapping. The scanning electron microscope (SEM) (Quanta 3D model, FEI, Inc.) combined with an EDAX X-ray spectrometer and a Si(Li) detector with a 10 mm^2 active area and an ATW2 window[6,56] was used to determine the size, morphology, and elemental composition of individual particles. Particles collected on the thin carbon-film substrates were identified and imaged using a mixed TE/BSE signal. Then, the X-ray spectrum for each identified particle was acquired at an acceleration voltage of 20 kV and a beam current of 430 pA for 10 s. Elemental compositions and equivalent circle diameters of individual particles were determined from the recorded X-ray spectra and images, respectively. Particle composition is reported in terms of atomic fractions and their ratios. More details on CCSEM/EDX analysis and X-ray mapping of individual particle are reported elsewhere.[57,58]

2.3. Micro-FTIR analysis. This analysis was used to identify the functional groups in particle samples. Detailed description of the micro-FTIR apparatus are reported elsewhere.[59,60] Briefly, the micro-FTIR setup consists of a Bruker A590 IR optical microscope, a Bruker IFS66/S FTIR spectrometer, and a mercury−cadmium−telluride detector. Particle samples collected on a SiN_x window were placed into a sealed environmental sample stage attached to the optical microscope. The sample stage allows the IR beam to pass through the particle sample. The IR beam was positioned to pass through the particle sample by moving the sample within the stage. All spectra were acquired in transmission mode by coadding 512 scans between 500 and 4000 cm^{-1} with 4 cm^{-1} spectral resolution. Background spectra were collected using a separate particle-free SiN_x "reference" window. For each sample, five background spectra were averaged and used as a reference spectrum. For the particle samples, an average of 15 spectra was used for further data analysis. All spectra were acquired using a 0.3 mm aperture at 295 ± 0.5 K under dry conditions (RH <10%). All sample spectra represent an ensemble of several hundreds of particles.

2.4. STXM/NEXAFS Analysis. STXM utilizes a focused soft X-ray beam generated from the synchrotron light source to probe functional groups within individual particles. By raster scanning the sample at fixed photon energy, images are obtained. Spatially resolved X-ray spectra are measured as a function of photon energy over the sample area. Particle mixing state and the chemical composition of individual particles at ~35 nm size resolution can be identified by analyzing the recorded spectra. A recent review provides an overview of the application of this technique to atmospheric aerosols[61] and technical details on STXM are published elsewhere.[61−64] STXM/NEXAFS measurements were conducted at beamline 11.0.2 of the Advanced Light Source in Lawrence Berkeley National Laboratory.

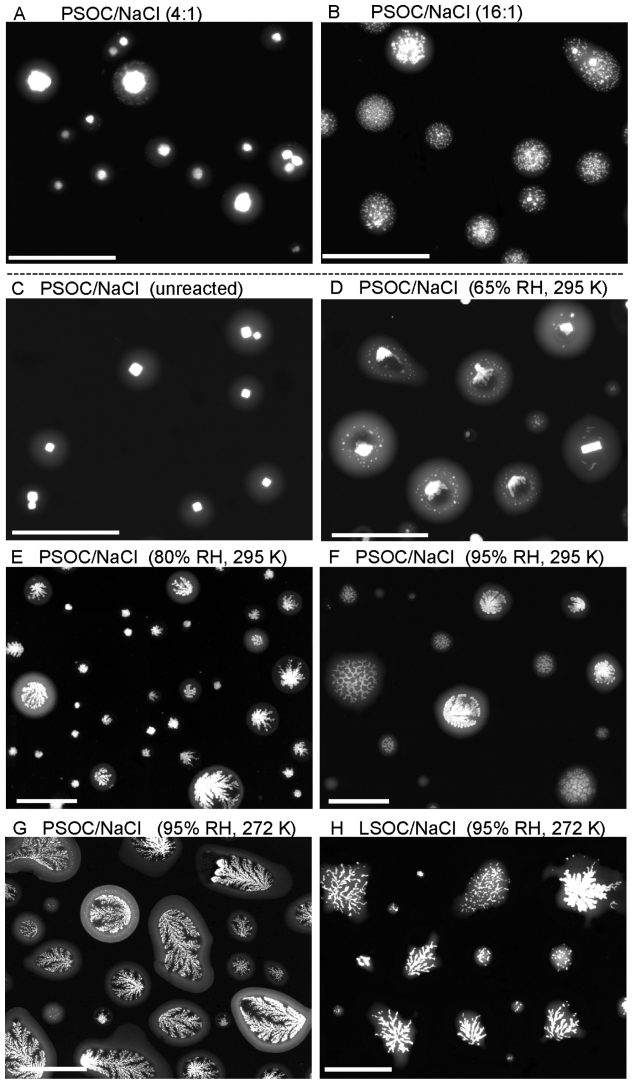

Figure 2. Characteristic SEM images of internally mixed PSOC/NaCl particles generated from solutions of 4:1 (A) and 16:1 (B) mass ratio; unreacted PSOC-coated NaCl particles (generated at dry conditions without further hydration/dehydration process) (C); PSOC-coated NaCl particles after exposure to 65%, 80%, and 95% RH at 295 K for 24 h (D−F); PSOC-coated and LSOC-coated NaCl particles after exposure to 95% RH at 272 K for 24 h (G,H). Size bar is 2 μm for all images.

2.5. Nano-DESI/HRMS. LSOC and PSOC samples were analyzed using a LTQ-Orbitrap high resolution mass spectrometer (Thermo Electron, Bremen, Germany) equipped with a custom built Nanospray Desorption Electrospray Ionization Source (nano-DESI).[65,66] The mass spectrometer was operated in the positive-ion mode with a resolving power of 100 000 at m/z 400. Analysis of the LSOC and PSOC samples deposited on the PTFE membranes was performed by bringing the sample in contact with the nano-DESI probe. Mass spectra were subsequently obtained by averaging the signal over the time window during which the nano-DESI probe was in contact with the SOC sample. HRMS data were analyzed as described in previous studies.[67,68]

dx.doi.org/10.1021/jp510336q | J. Phys. Chem. A 2015, 119, 4498−4508

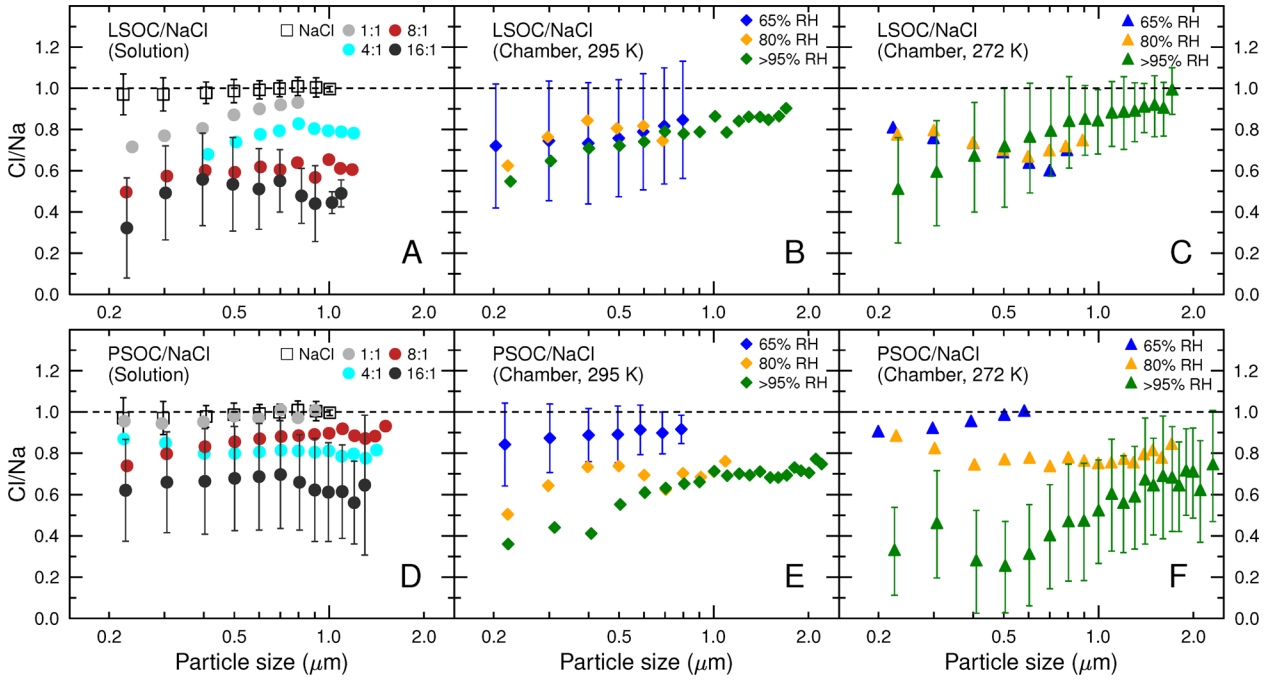

Figure 3. Mean Cl/Na atomic ratios for LSOC/NaCl (A,B,C) and PSOC/NaCl (D,E,F) particles determined by CCSEM/EDX analysis. Panels A and D are for particles generated from solutions with mass ratios (SOC:NaCl) at 1:1 (gray), 4:1 (cyan), 8:1 (brown), and 16:1 (black); Panels B, C, E, and F are for SOC-coated NaCl particles after exposure to water vapor at 95% (green), 80% (orange), and 65% RH (blue) at 295 K (B,E) and 272 K (C,F) for 24 h, respectively. Reference Cl/Na data for pure NaCl particles are shown in panels A and D (open squares). Dashed lines indicate the nominal Cl/Na = 1 ratio if no chloride depletion occurs. Representative uncertainties (one standard deviation) are shown in each panel. Uncertainties for other data sets (omitted for clarity) are similar to the representative uncertainties.

3. RESULTS AND DISCUSSION

3.1. Reactions of SOC with NaCl and $NaNO_3$. For the first set of experiments, the effect of SOC fraction on the reaction extent was investigated. Internally mixed particles were generated by nebulizing the solutions at different SOC/NaCl mass ratios and then dehydrated before analysis. Figures 2A,B and S2 show typical SEM images for these dehydrated particles. Na-containing components (brighter part of the particles shown in SEM images) are mixtures of NaCl and sodium organic salts (see later discussion on the organic salt formation). Particle morphology demonstrates the mixing state of Na-containing components and SOC after dehydration. At lower SOC fractions, NaCl remains relatively intact. With increasing SOC fractions, particle morphology changes dramatically, indicating substantial reaction between NaCl and SOC and that the particle composition changes after reaction. Figures 3A,D show Cl/Na atomic ratios in internally mixed SOC/NaCl particles determined by CCSEM/EDX analysis. Cl/Na ratios decrease from ~0.95 to 0.3 as LSOC/NaCl and PSOC/NaCl mass ratios (in the original solutions) increase from 1:1 to 16:1. Chloride depletion is due to acid displacement by organic acid in SOC through reaction R1 and results in the evaporation of HCl after dehydration. Higher SOC content provides more HA(org) to displace HCl and results in greater chloride depletion. In general, at the same mass ratios, LSOC depletes chloride more effectively than PSOC. This is consistent with LSOC having a relatively higher organic acid content than PSOC (SI text and Figure S3). In addition, chloride depletion by LSOC is higher in smaller particles, while chloride depletion due to PSOC exhibits no significant size dependence.

For the second set of experiments, the reactions of particles with core/shell structures were investigated. Crystalline NaCl particles were coated with SOC in an environmental chamber under dry conditions and then collected on substrates (thereafter referred to as "SOC-coated particles"). Multiple particle samples were separately exposed to 65%, 80%, and 95% RH at 295 and 272 K for 24 h and then dehydrated prior to analysis. SEM images of Figure 2C−H and Figure S2 show that the morphology for these reacted and dehydrated particles is dramatically changed by exposure to the different RH and temperatures. These variations in particle morphology indicate different extents of interactions/reactions. For PSOC-coated particles, the inclusions change from cubic shapes (unreacted NaCl cores, Figure 2C), to relatively intact (65% RH, Figure 2D), and to distinct fractal structures (80% RH, Figure 2E; 95% RH, Figure 2F,G). Similar trends in morphological changes were observed for LSOC-coated particles (Figures 2H and S2). Significant chloride depletion by LSOC and PSOC (up to 80% with Cl/Na ratio of ~0.2) was observed (Figure 3B,C,E,F). Within the experimental uncertainties, temperature and RH dependences were observed for the chloride depletion by PSOC, but not for LSOC. PSOC-coated particles exposed to higher RH before dehydration and analysis have enhanced chloride depletion. Smaller particles have higher chloride depletion.

The time dependence of the reactions was also examined. PSOC-coated particles were exposed to water vapor at 95% RH and 295 K for 8, 16, and 25 h and then dehydrated prior to analysis. Size and reaction time dependences for chloride depletion by PSOC were observed as shown in Figure 4. Greater depletion was observed for smaller particles and for longer reaction times. Cl/Na ratios down to 0.8, 0.5, and 0.25 were measured when particles were exposed for 8, 16, and 25 h,

dx.doi.org/10.1021/jp510336q | J. Phys. Chem. A 2015, 119, 4498−4508

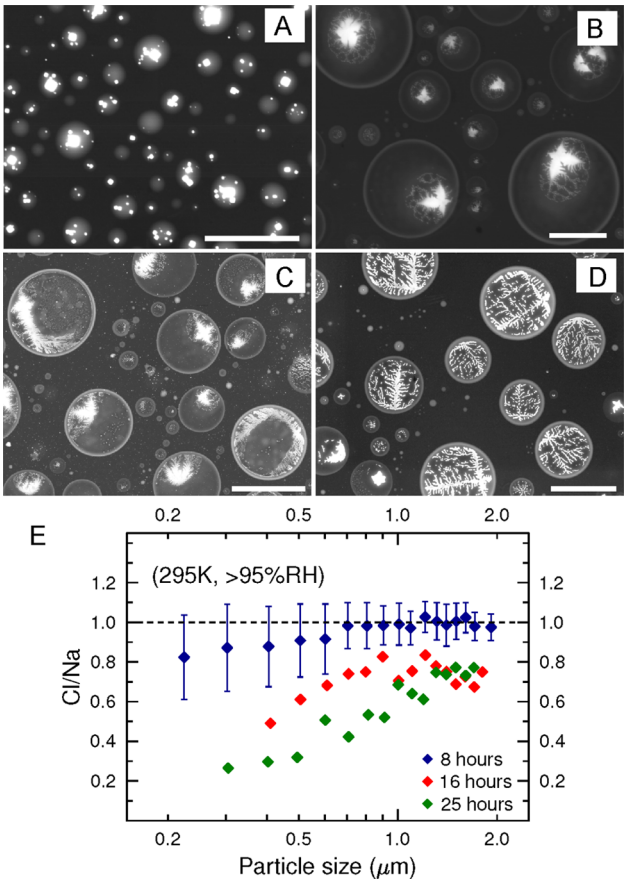

Figure 4. Time dependence of chloride depletion by PSOC. (A) SEM image for PSOC-coated NaCl particles before exposure to water vapor. (B,C,D) SEM images for particles after 8 (B), 16 (C), and 25 (D) hour reaction times. (E) Mean atomic ratios of Cl/Na as a function of particle size for PSOC-coated NaCl particles exposed to 95% RH at 295 K for 8, 16, and 25 h. Dashed lines indicate the nominal Cl/Na ratio of 1 if no chloride depletion occurs. Representative uncertainties (one standard deviation) are shown. Size bar is 3 μm for all the images.

respectively. For 8 h exposure times, the fractal-like inclusions were observed within the central part of the individual particles. For longer exposures, 16 and 25 h, the fractal-like inclusions were distributed throughout the particles, indicating more extensive reaction as compared to particles with shorter exposures (i.e., 8 h).

For most of the investigated particles including those exposed to RH higher than 80%, the inclusions are often located in the particle center after dehydration. You et al. (2014) showed that liquid−liquid phase separation was typically observed in organic/inorganic particles including organic/NaCl mixtures when the O:C of organic species is less than 0.5.[69] Based on the nano-DESI/HRMS analysis, the estimated average O:C ratio for LSOC and PSOC in this study is 0.46 and 0.37, respectively. Thus, liquid−liquid phase separation most likely also occurred for the particles upon drying. The inorganic core and organic shell might then act as a template for the observed structure after efflorescence. In addition, the dendritic morphology of NaCl or organic sodium salt inclusions is likely a result of slow crystallization in the viscous particles upon dehydration. This is consistent with increasing viscosity of SOC at lower RH, as will be discussed in a later section.

Figure 5A−C shows elemental maps of the reacted PSOC-coated particles. For the reacted particles, particle shells contain

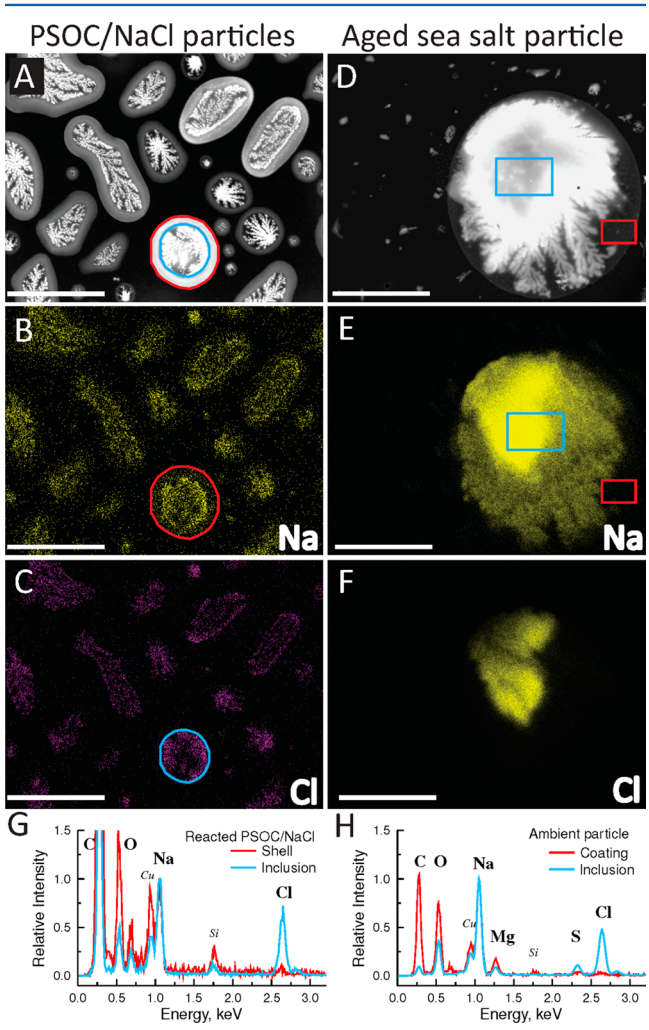

Figure 5. SEM images and elemental (Na and Cl) mapping for PSOC-coated NaCl particles exposed to 95% RH at 272 K (A−C) and for a typical ambient particle collected during the CARES campaign (D−F). Panel G shows the spectra for the shell (between red and blue circles in SEM image) and inclusion (inside blue circle) of a reacted PSOC/NaCl particle. Panel H shows the spectra for the coating (blue box) and inclusion (red box) of the ambient aged sea salt particle. All X-ray intensities are normalized to the intensity of Na peak. Size bar is 2 μm for all images.

substantial amounts of Na with nearly complete chloride depletion, whereas the fractal-like inclusions are not as depleted in chloride, as indicated by the corresponding X-ray spectra shown in Figure 5G. This indicates that the particle shells most likely consist of SOC and sodium organic salts. This finding is corroborated by STXM and micro-FTIR analyses, as will be discussed later. Similar observations were also found in the reacted LSOC-coated particles (Figure S4). Figure 5D−F and Figure S5 illustrate aged sea salt particles collected during the Carbonaceous Aerosols and Radiative Effects Study (CARES) in Central California, where a significant fraction (~60%−70%) of chloride depletion was attributed to acid displacement by organic acids.[43] The total chloride depletion in the organic coating of these particles, without the presence of sulfate or nitrate, indicates the reactions between sea salt and organic materials (Figure S5). In comparison, SOC (which contains

dx.doi.org/10.1021/jp510336q | J. Phys. Chem. A 2015, 119, 4498−4508

organic acids) can react with NaCl and results in morphologies and chloride depletion similar to that observed in the atmospheric aged particles with secondary organic coatings.

3.2. STXM and Micro-FTIR Characterization. STXM/NEXAFS analysis provided imaging of sodium and carbon chemical bonding and mixing states of individual particles.[62,70] Figure 6A–C shows characteristic carbon K-edge maps of the

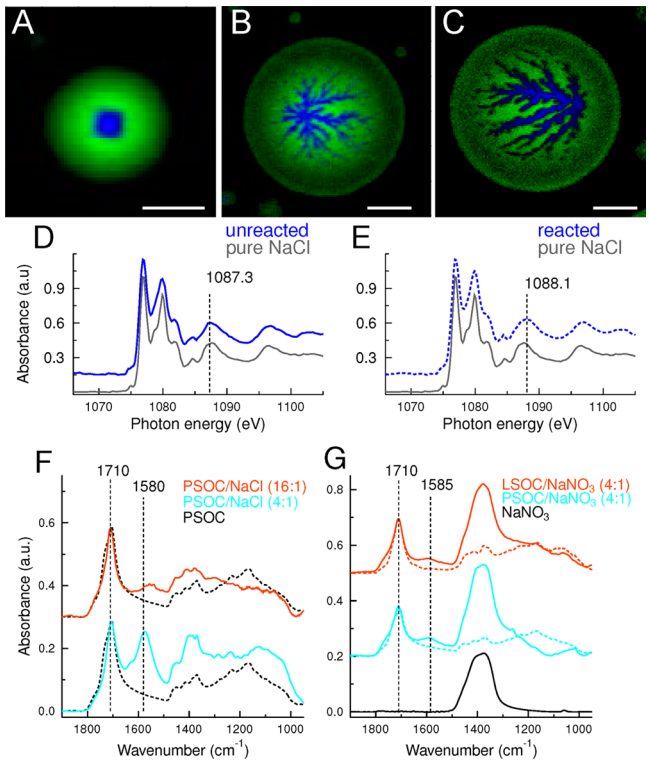

Figure 6. Representative compositional mappings of unreacted (A) and reacted (B,C) PSOC/NaCl particles determined by STXM/NEXAFS using carbon K-edge spectra. Inorganic and organic components are indicated in blue and green, respectively. (D,E) Na K-edge NEXAFS spectra for inclusions in unreacted and reacted PSOC/NaCl particles with reference spectrum of pure NaCl. Micro-FTIR spectra for PSOC/NaCl particles at 4:1 (cyan) and 16:1 (red) mass ratios (F) and LSOC/$NaNO_3$ (cyan) and PSOC/$NaNO_3$ (red) particles at 4:1 mass ratio (G). Reference FTIR spectra are shown for LSOC (dash lines), PSOC (dash lines), and $NaNO_3$ (black line).

COOH functional group (organic, green area) and inorganic material (blue area) for unreacted and reacted PSOC-coated NaCl particles. The morphology and mixing state of different components are consistent with SEM/EDX analysis. The STXM/NEXAFS measurements indicate the presence of a small amount of Na and reduced Cl in the organic coating, before and after reaction, and are also consistent with SEM/EDX analysis. Figure 6D,E show the Na K-edge NEXAFS spectra for the NaCl inclusions (blue areas in Figure 6A,C) in unreacted and reacted particles, respectively. The shift of the 1087.3 eV peak to 1088.1 eV is attributed to a reduction in the Na–Cl bond length.[70] Removing Cl from the particles (organic matrix) via reaction may introduce defects into the NaCl inclusions and reduce the Na–Cl average bond length since the ionic radius of Cl^- is larger than that of Na^+.

Formation of NaA(org) salts was apparent in micro-FTIR spectra acquired over large ensembles of reacted SOC/NaCl particles. Figure 6F shows spectra corresponding to the reacted PSOC-coated NaCl particles plotted along with the reference spectrum of pure PSOC. A common feature of carboxylic acids (–COOH functional group at ~1710 cm^{-1}) is prominent in all the spectra. PSOC/NaCl particles reacted at 4:1 and 16:1 mass ratios display a new strong feature characteristic of carboxylate (COONa) at ~1580 and ~1585 cm^{-1}, respectively. The red shift for the higher PSOC/Na mass ratios indicates stronger interactions between PSOC and the NaCl/HA(org) salt. Similar results were also obtained for LSOC/NaCl particles (Figure S6). To investigate the reaction between SOC and $NaNO_3$, SOC/$NaNO_3$ particles generated from solutions were analyzed by micro-FTIR after dehydration. Figure 6G show that SOC/$NaNO_3$ particles have a characteristic carboxylate peak at ~1585 cm^{-1}, indicating the reaction between organic acids and $NaNO_3$ and the formation of organic salts during dehydration processes.

3.3. Effects of SOC Viscosity on Its Reactivity. Previous studies showed that PSOC may adopt liquid, semisolid, and solid states[22,27,33] which could affect the uptake of reactive gases such as NH_3.[25] To better understand the role of particle phase states on the reactivity of SOC with chloride and nitrate, T_g for PSOC as a function of RH, T_g(RH), was estimated based on the methods presented in previous studies[6,13] using the following equations:

$$T_g = \frac{m_w \times T_{g,w} + m_{org} \times \frac{T_{g,org}}{k_{GT}}}{m_w + \frac{m_{org}}{k_{GT}}} \quad (1)$$

$$\frac{RH}{100} = a_w = \left(1 + \kappa_{org}\frac{\rho_w}{\rho_{org}}\frac{m_{org}}{m_w}\right)^{-1} \quad (2)$$

where m_i, ρ_i, and $T_{g,i}$ are the mass fraction, density, and glass transition temperature of the pure component, respectively; the subscripts "w" and "org" refer to water and organic materials, respectively; k_{GT} is the Gordon–Tayler constant for the specific organic material representing the interaction between water and organic solute; and k_{org} is the hygroscopicity parameter of the organic component. Based on eqs 1 and 2, T_g(RH) can be expressed as

$$T_g(RH) = \frac{T_{g,w} \times k_{GT} + f(RH) \times T_{g,org}}{k_{GT} + f(RH)} \quad (3)$$

where

$$f(RH) = \frac{m_{org}}{m_w} = \frac{100 - RH}{RH}\frac{1}{\kappa_{org}}\frac{\rho_{org}}{\rho_w} \quad (4)$$

First, with the assumption of PSOC adopting solid state at 293 ± 1 K and 35 ± 5% RH,[22] the $T_{g,org}$ for pure PSOC was estimated as 310 ± 15 K ranging from 295 to 328 K. k_{GT}, κ_{org}, ρ_{org}, ρ_w of 2.5 ± 1.0,[6,13,36,71] 0.1 ± 0.04,[72,73] 1.4 ± 0.2 g cm^{-3},[53] and 1.0 g cm^{-3} were used, respectively. The estimated T_g of 310 ± 15 K at 0% RH for PSOC is close to the upper value of 328 ± 13 K predicted by Berkemeier et al.[28] Then, T_g(RH) was derived using eq 3 and constrained by $T_{g,org}$ of 310 K (at 0% RH) and $T_{g,w}$ of 136 K (at 100% RH). Here we assume that a_w does not change significantly for constant solution composition with decreasing temperature.[74] Figure 7A shows T–RH phase diagrams for PSOC. The black line shows T_g(RH) for PSOC with $T_{g,org}$, k_{GT}, κ_{org}, ρ_{org}, of 310 K, 3.5, 0.1, and 1.4 g cm^{-3}, respectively. T_g(RH) reported here should be treated as an

dx.doi.org/10.1021/jp510336q | J. Phys. Chem. A 2015, 119, 4498–4508

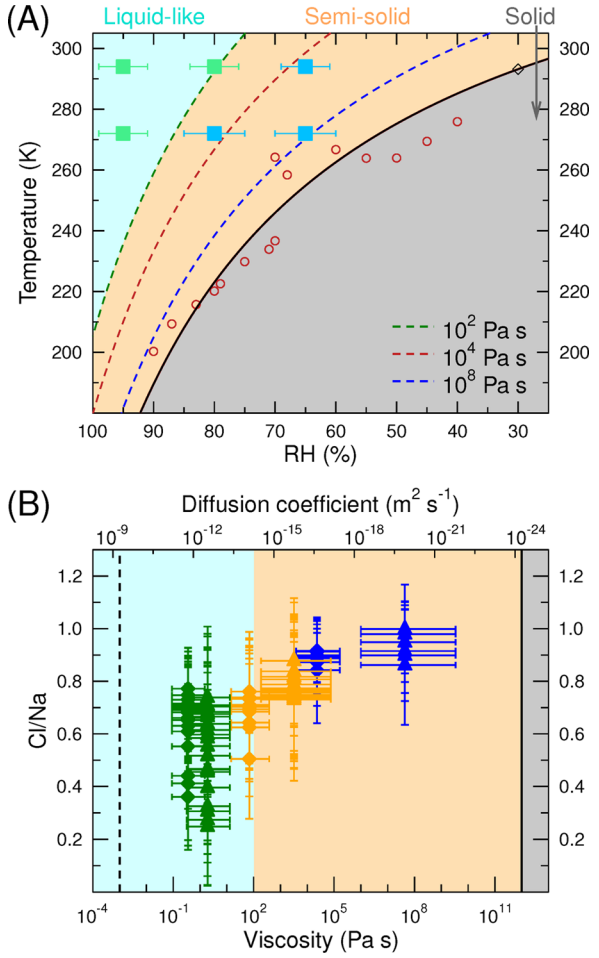

Figure 7. (A) Estimated η of PSOC as a function of temperature and RH. Dashed lines indicate η of 10^2 (green), 10^4 (brown), and 10^8 (blue) Pa s. Solid squares indicate η at temperature and RH values of this study, where PSOC is estimated to be in liquid-like (light green) and semisolid (light blue) states. Black line indicates the T_g (RH) of PSOC (η = 10^{12} Pa s). Circles indicate the estimated T_g of PSOC derived from the reported η at ~293 K by Renbaum-Woff et al.[22] and assuming T_g of 293 K at 30% RH (open diamond). (B) Cl/Na ratios reported in Figure 3E,F for reacted PSOC/NaCl particles as a function of η for PSOC at 295 K (diamonds) and 272 K (triangles), at 65% (blue), 80% (orange), and 95% RH (green). Dashed and solid lines indicate η of pure water and solids (at η = 10^{12} Pa s), respectively. Gray, tan, and cyan areas indicate the temperature and RH conditions when PSOC is in solid (η > 10^{12} Pa s), semisolid (10^2 Pa s < η < 10^{12} Pa s), and liquid-like (η < 10^2 Pa s) states, respectively.

upper limit. Abramson et al., (2013) estimated the PSOC viscosity to be higher than 10^8 Pa s based on the evaporation experiments at dry condition and room temperature.

Based on the T_g(RH) estimated above, the temperature dependence of viscosity for PSOC was calculated by the Williams–Landel–Ferry equation:[75,76]

$$\log(\eta(T, \mathrm{RH})) = \log(\eta_{T_g}) + \frac{-17.44(T - T_g(RH))}{51.6 + T - T_g(RH)} \quad (5)$$

where η(T,RH) is the viscosity at T and RH, and η_{Tg} of 10^{12} Pa s is the viscosity at the glass transition points, T_g(RH). The constant η value of 10^2, 10^4, and 10^8 Pa s for PSOC are also shown in Figure 7A. To validate this approach, the estimated η for PSOC in this study are compared to experimentally determined η by Renbaum–Wolff et al.[22] at 293–295 K. As shown in Figure 8, the estimated η here are in consistent with

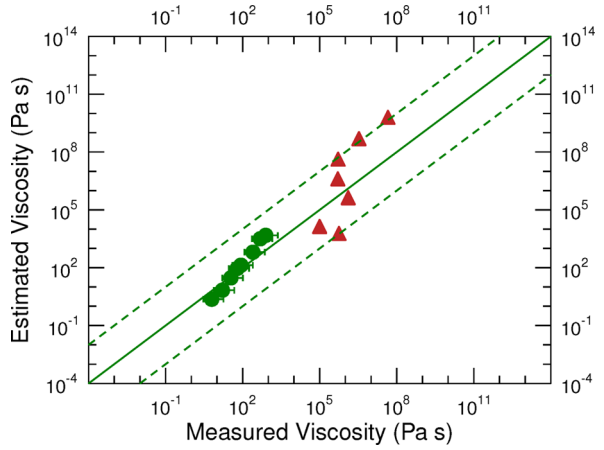

Figure 8. Comparison of estimated viscosity from this study with measured viscosity by Renbaum-Wolff et al.[22] Circles and triangles indicate the mean and upper limit of viscosity measured by Renbaum-Wolff et al.[22] using "bead-mobility" (circle, at >70%RH) and "poke-flow" (triangles, at <70% RH) techniques, respectively. Solid and dashed lines indicate 1:1 and 2 orders of magnitude differences, respectively.

the measured η by Renbaum–Wolff et al.[22] Alternatively, one can calculate T_g reversely using the Williams–Landel–Ferry equation (eq 5) from the measured η. As shown in Figure 7, it is consistent with T_g(RH) estimated here using eqs 3 and 4. Figure 7A and Table 1 show the estimated T_g and η of PSOC under a range of RH and temperature pertinent to this study. T_g of PSOC decreases from 254.8 K at 65% RH to 166.3 K at 95% RH. η of PSOC changes from ~4.0 × 10^{-1} (95% RH) to 3.0 × 10^4 Pa s (65% RH) and from ~1.9 × 10° (95% RH) to 4.4 × 10^7 Pa s (65% RH) at 295 and 272 K, respectively. Under our experimental conditions, when the PSOC-coated NaCl particles were exposed to water vapor PSOC was either liquid (η < 10^2 Pa s) or semisolid (10^2 Pa s < η < 10^{12} Pa s).

Estimated viscosity values were used to calculate the self-diffusion coefficient (D_{org}) and e-folding time of equilibration (τ_e) for PSOC molecular transport or mixing within particles. D_{org} of organic species within a liquid or semisolid particle (organic matrix) can be calculated using the Stokes–Einstein equation: $D_{org} = k_B T/(6\pi\alpha\eta)$, where k_B is the Boltzmann constant, T is the temperature, α is the estimated PSOC molecular radius of ~0.38 nm,[22] and η is the viscosity of the particle derived in this study. τ_e showing the time of mass-transport or mixing by molecular diffusion within the particles can be estimated according to $\tau_e = d_p^2/4\pi^2 D$, where d_p is the particle diameter and D is the diffusion coefficient of the molecule.[18] Table 1 lists the D_{org} for PSOC at the investigated experimental conditions. The τ_e for transport or mixing of PSOC within a particle of 2 μm in diameter are also listed in Table 1.

D_{org} of 1.20 × 10^{-20} and 2.46 × 10^{-17} m^2 s^{-1} with corresponding τ_e of 2344 and 1.1 h were estimated for PSOC at 65% RH at 272 and 295 K, respectively. Characteristic τ_e for particles reacted at higher RH conditions are less than 0.2 h. Diffusion coefficients for small molecules (such as H_2O and HCl) are often several orders of magnitude higher than self-diffusion of PSOC within a semisolid organic matrix.[16,37] For example, D_{H2O} ranges from 10^{-17} to 10^{-8} m^2 s^{-1} in glassy and

dx.doi.org/10.1021/jp510336q | J. Phys. Chem. A 2015, 119, 4498–4508

Table 1. Estimates of Glass Transition Temperature (T_g), Viscosity (η), Self-Diffusion Coefficient (D_{org}), and e-Folding Time of Equilibration (τ_e, for particles of 2 μm in diameter) for PSOC at the Investigated Experimental Conditions

		η (Pa s)		D_{org} (m^2 s^{-1})		τ_e (hour)	
RH (%)	T_g (K)	295 K	272 K	295 K	272 K	295 K	272 K
65	254.8	3.0×10^4	4.4×10^7	2.46×10^{-17}	1.20×10^{-20}	1.1	2344
80	223.0	8.0×10^1	3.2×10^3	8.20×10^{-15}	1.64×10^{-16}	~0[a]	0.2
95	166.3	4.0×10^{-1}	1.9×10^0	1.60×10^{-12}	2.74×10^{-13}	~0[a]	~0[a]

[a]The τ_e is less than 1 min.

liquid organic matrix with a_w higher than 0.2.[36,37,77−79] Since the experiments were performed at a specific RH for 24 h above 272 K, the diffusion of H_2O/HCl is not expected to be the factor limiting the reaction. However, self-diffusion of PSOC may hinder the reaction with NaCl for particles with initial core(NaCl)/shell(PSOC) structures. Figure 7B shows that Cl/Na ratios for reacted PSOC/NaCl particles (Figure 3E,F) increase at higher viscosities (i.e., > 10^2 Pa s) indicating less chloride depletion. Thus, particle viscosity may have significant effects on the acid displacement reaction. For example, no chloride depletion was observed at 272 K and 65% RH when η is 4.4×10^7 Pa s, whereas at 295 K and 95% RH when η is 0.4 Pa s chloride was significantly depleted. Currently, no data are available for accurate estimates of T_g(RH) for LSOC. Since the oxidation state of LSOC is somewhat higher than PSOC (SI text) and LSOC is more hygroscopic, T_g(RH) of LSOC is likely lower than PSOC at high RH[13]. Therefore, LSOC may be less viscous than PSOC under the investigated conditions and self-diffusion of LSOC would have less effect on the reaction. Thus, the Cl/Na ratios reported for LSOC/NaCl particles did not exhibit a strong RH dependence (Figure 3). It is worth noting that the limited water content available in the particles is also a critical factor controlling the reaction at lower RH.

For particles that are in a liquid-like state, the relatively short τ_e shows that the reaction should not be hindered by the diffusion of PSOC, water, or HCl (Table 1). While this indicates that chloride depletion by PSOC should be time-independent during the time scale of our experiments at high RH conditions, we observed higher chloride depletion for longer reaction times at 295 K and 95% RH (Figure 4). One explanation is that the reaction may also be controlled by the slowly evolving content of hydrolyzed PSOC material. This is likely a result of low acid dissociation constants of HA(org) present in fresh PSOC that do not produce enough protons to complete reaction R1. As PSOC interacts with water its constituents are slowly hydrolyzed to produce smaller acids[27,80,81] that continue to dissociate during the course of the experiments (24 h) providing more protons for the reaction. Further studies on the reaction kinetics are needed.

4. SUMMARY AND IMPLICATIONS

This work shows that condensed-phase SOC from ozonolysis of limonene and α-pinene reacts with NaCl in aerosol particles through acid displacement by organic acids. This reaction is driven by the volatile HCl product degassing from aerosol particles resulting in the release of gaseous HCl and formation of organic salts. Substantial chloride depletion and particle morphology changes were observed for SOC/NaCl particles at various atmospherically relevant conditions. The reactions are expected to hold for organic acids produced from other major types of biogenic and anthropogenic SOC precursors as well as other inorganic species. Analogous reactions are expected in mixed SOC/$NaNO_3$ particles based on the pilot FTIR data presented here (Figure 6F) and in our previous work where reactions R2 of selected HA(org)/$NaNO_3$ and HA(org)/$Ca(NO_3)_2$ mixed particles were reported.[44] We showed that low molecular weight water-soluble carboxylic acids can deplete nitrate through similar reactions.[44] Similar reactions were also reported for internally mixed particles containing calcite components of mineral dust and condensed phase organic acids.[48] The release of HCl and HNO_3 from these reactions can affect their gas-particle partitioning and react with other atmospheric constituents, such as mineral dust. Potential recycling of HCl and HNO_3 may alter the related atmospheric chemistry, for example, the continental and marine nitryl chloride formation.[82] Formation of organic salts, likely with low volatility and reduced solubility,[44,50] could change the partitioning of organic acids in gas and condensed phase and thus affect the formation and atmospheric evolution of SOC. The resulting organic salts can contribute to a significant fraction of particle mass and may change particle composition, hygroscopicity,[46,47,51] CCN activity,[50,83] reactivity, optical properties, and ice nucleation ability.[84]

Glass transition temperatures and viscosity of PSOC as a function of temperature and RH were estimated. Depending on reaction time and particle size, self-diffusion of PSOC within highly viscous or semisolid particles can hinder the reaction extent at low temperatures and RH. The phase state of not only SOC but also inorganics such as metastable viscous brines of $NaNO_3$ and $Ca(NO_3)_2$ at low RH[44,59] can affect the reactions. The results indicate that reaction of SOC with NaCl is a dynamic process, and its extent is influenced by SOC composition, phase state and viscosity, temperature, RH, and particle size. The estimated glass transition temperatures and viscosity for SOC can also be used to determine the diffusivities of water, oxidants, or organic molecules that in turn will influence water uptake, SOC formation, and heterogeneous reactions within or on the particle surfaces at atmospherically relevant temperature and humidity. Further experimental and modeling studies are needed on the reactivity of SOC from different precursors, reaction kinetics, other controlling factors on these reactions, and potential atmospheric impacts.

■ ASSOCIATED CONTENT

Supporting Information

Supporting Information includes the following materials: estimates of the SOC/NaCl mass ratios for the investigated particles and estimates of average O/C ratio of SOC; schematics of the setup for water vapor exposure experiments; additional SEM images, X-ray mapping, and micro-FTIR spectra of particles. This material is available free of charge via the Internet at http://pubs.acs.org.

dx.doi.org/10.1021/jp510336q | J. Phys. Chem. A 2015, 119, 4498−4508

AUTHOR INFORMATION

Corresponding Authors

*E-mail: Bingbing.Wang@pnnl.gov (B.W.).
*E-mail: Alexander.Laskin@pnnl.gov (A.L.).

Notes

The authors declare no competing financial interest.

ACKNOWLEDGMENTS

B.W., A.L., and J.E.S. acknowledge support from the Chemical Imaging Initiative of the Laboratory Directed Research and Development program at Pacific Northwest National Laboratory (PNNL). The CCSEM/EDX, micro-FTIR, and nano-DESI/HRMS analyses were performed at Environmental Molecular Sciences Laboratory, a national scientific user facility sponsored by OBER at PNNL. PNNL is operated by the U.S. Department of Energy by Battelle Memorial Institute under contract DE-AC06-76RL0. STXM/NEXAFS analysis at beamline 11.0.2 of the Advanced Light Source at Lawrence Berkeley National Laboratory is supported by the Director, Office of Science, Office of Basic Energy Sciences of the U.S. Department of Energy under Contract No. DE-AC02-05CH11231. M.K.G., S.T.K., and Beamline 11.0.2 also acknowledge support from the Office of Basic Energy Sciences Division of Chemical Sciences, Geosciences, and Biosciences by the Condensed Phase and Interfacial Molecular Sciences Program of the U.S. Department of Energy. Sample collection during CARES field study and postdoctoral support for REO were provided by the Atmospheric System Research (ASR) Program sponsored by the U.S. Department of Energy (DOE), Office of Science, Office of Biological and Environmental Research (OBER).

REFERENCES

(1) Ramanathan, V.; Crutzen, P. J.; Kiehl, J. T.; Rosenfeld, D. Aerosols, Climate, and the Hydrological Cycle. *Science* **2001**, *294*, 2119−2124.

(2) Forster, P.; Ramaswamy, V.; Artaxo, P.; Berntsen, T.; Betts, R. *Climate Change 2007: The Physical Science Basis*; Contribution of Working Group I to the Fourth Assessment Report of the Intergovernmental Panel on Climate Change; Cambridge University Press: Cambridge, New York, 2007.

(3) Pöschl, U. Atmospheric Aerosols: Composition, Transformation, Climate and Health Effects. *Angew. Chem., Int. Ed.* **2005**, *44*, 7520−7540.

(4) Rosenfeld, D. Suppression of Rain and Snow by Urban and Industrial Air Pollution. *Science* **2000**, *287*, 1793−1796.

(5) Baker, M. B. Cloud Microphysics and Climate. *Science* **1997**, *276*, 1072−1078.

(6) Wang, B.; Lambe, A. T.; Massoli, P.; Onasch, T. B.; Davidovits, P.; Worsnop, D. R.; Knopf, D. A. The Deposition Ice Nucleation and Immersion Freezing Potential of Amorphous Secondary Organic Aerosol: Pathways for Ice and Mixed-Phase Cloud Formation. *J. Geophys. Res.: Atmos.* **2012**, *117*, D16209.

(7) Hoose, C.; Möhler, O. Heterogeneous Ice Nucleation on Atmospheric Aerosols: A Review of Results from Laboratory Experiments. *Atmos. Chem. Phys.* **2012**, *12*, 9817−9854.

(8) Knopf, D. A.; Wang, B.; Laskin, A.; Moffet, R. C.; Gilles, M. K. Heterogeneous Nucleation of Ice on Anthropogenic Organic Particles Collected in Mexico City. *Geophys. Res. Lett.* **2010**, *37*, L11803.

(9) Pöschl, U.; Martin, S. T.; Sinha, B.; Chen, Q.; Gunthe, S. S.; Huffman, J. A.; Borrmann, S.; Farmer, D. K.; Garland, R. M.; Helas, G.; et al. Rainforest aerosols as biogenic nuclei of clouds and precipitation in the Amazon. *Science* **2010**, *329*, 1513−1516.

(10) Zhang, Q.; Jimenez, J. L.; Canagaratna, M. R.; Allan, J. D.; Coe, H.; Ulbrich, I.; Alfarra, M. R.; Takami, A.; Middlebrook, A. M.; Sun, Y. L.; et al. Ubiquity and dominance of oxygenated species in organic aerosols in anthropogenically-influenced Northern Hemisphere midlatitudes. *Geophys. Res. Lett.* **2007**, *34*, L13801.

(11) Jimenez, J. L.; Canagaratna, M. R.; Donahue, N. M.; Prevot, A. S. H.; Zhang, Q.; Kroll, J. H.; DeCarlo, P. F.; Allan, J. D.; Coe, H.; Ng, N. L.; et al. Evolution of organic aerosols in the atmosphere. *Science* **2009**, *326*, 1525−1529.

(12) Kanakidou, M.; Seinfeld, J. H.; Pandis, S. N.; Barnes, I.; Dentener, F. J.; Facchini, M. C.; Van Dingenen, R.; Ervens, B.; Nenes, A.; Nielsen, C. J.; et al. Organic aerosol and global climate modelling: A review. *Atmos. Chem. Phys.* **2005**, *5*, 1053−1123.

(13) Koop, T.; Bookhold, J.; Shiraiwa, M.; Poschl, U. Glass Transition and Phase State of Organic Compounds: Dependency on Molecular Properties and Implications for Secondary Organic Aerosols in the Atmosphere. *Phys. Chem. Chem. Phys.* **2011**, *13*, 19238−19255.

(14) Virtanen, A.; Joutsensaari, J.; Koop, T.; Kannosto, J.; Yli-Pirilae, P.; Leskinen, J.; Maekelae, J. M.; Holopainen, J. K.; Poeschl, U.; Kulmala, M.; et al. An amorphous solid state of biogenic secondary organic aerosol particles. *Nature* **2010**, *467*, 824−827.

(15) Zhou, S.; Shiraiwa, M.; McWhinney, R. D.; Poschl, U.; Abbatt, J. P. D. Kinetic Limitations in Gas-Particle Reactions Arising from Slow Diffusion in Secondary Organic Aerosol. *Faraday Discuss.* **2013**, *165*, 391−406.

(16) Shiraiwa, M.; Zuend, A.; Bertram, A. K.; Seinfeld, J. H. Gas-Particle Partitioning of Atmospheric Aerosols: Interplay of Physical State, Non-Ideal Mixing and Morphology. *Phys. Chem. Chem. Phys.* **2013**, *15*, 11441−11453.

(17) Shiraiwa, M.; Yee, L. D.; Schilling, K. A.; Loza, C. L.; Craven, J. S.; Zuend, A.; Ziemann, P. J.; Seinfeld, J. H. Size Distribution Dynamics Reveal Particle-Phase Chemistry in Organic Aerosol Formation. *Proc. Natl. Acad. Sci. U.S.A.* **2013**, *110*, 11746−11750.

(18) Shiraiwa, M.; Ammann, M.; Koop, T.; Pöschl, U. Gas Uptake and Chemical Aging of Semisolid Organic Aerosol Particles. *Proc. Natl. Acad. Sci. U.S.A.* **2011**, *108*, 11003−11008.

(19) Pajunoja, A.; Malila, J.; Hao, L. Q.; Joutsensaari, J.; Lehtinen, K. E. J.; Virtanen, A. Estimating the Viscosity Range of SOA Particles Based on Their Coalescence Time. *Aerosol. Sci. Technol.* **2014**, *48*, I−IV.

(20) Vaden, T. D.; Imre, D.; Beranek, J.; Shrivastava, M.; Zelenyuk, A. Evaporation Kinetics and Phase of Laboratory and Ambient Secondary Organic Aerosol. *Proc. Natl. Acad. Sci. U.S.A.* **2011**, *108*, 2190−2195.

(21) Perraud, V.; Bruns, E. A.; Ezell, M. J.; Johnson, S. N.; Yu, Y.; Alexander, M. L.; Zelenyuk, A.; Imre, D.; Chang, W. L.; Dabdub, D.; et al. Nonequilibrium atmospheric secondary organic aerosol formation and growth. *Proc. Natl. Acad. Sci. U.S.A.* **2012**, *109*, 2836−2841.

(22) Renbaum-Wolff, L.; Grayson, J. W.; Bateman, A. P.; Kuwata, M.; Sellier, M.; Murray, B. J.; Shilling, J. E.; Martin, S. T.; Bertram, A. K. Viscosity of α-Pinene Secondary Organic Material and Implications for Particle Growth and Reactivity. *Proc. Natl. Acad. Sci. U.S.A.* **2013**, *110*, 8014−8019.

(23) Cappa, C. D.; Wilson, K. R. Evolution of Organic Aerosol Mass Spectra Upon Heating: Implications for OA Phase and Partitioning Behavior. *Atmos. Chem. Phys.* **2011**, *11*, 1895−1911.

(24) Abramson, E.; Imre, D.; Beranek, J.; Wilson, J.; Zelenyuk, A. Experimental Determination of Chemical Diffusion within Secondary Organic Aerosol Particles. *Phys. Chem. Chem. Phys.* **2013**, *15*, 2983−2991.

(25) Kuwata, M.; Martin, S. T. Phase of Atmospheric Secondary Organic Material Affects Its Reactivity. *Proc. Natl. Acad. Sci. U.S.A.* **2012**, *109*, 17354−17359.

(26) Loza, C. L.; Coggon, M. M.; Nguyen, T. B.; Zuend, A.; Flagan, R. C.; Seinfeld, J. H. On the Mixing and Evaporation of Secondary Organic Aerosol Components. *Environ. Sci. Technol.* **2013**, *47*, 6173−6180.

(27) Kidd, C.; Perraud, V.; Wingen, L. M.; Finlayson-Pitts, B. J. Integrating Phase and Composition of Secondary Organic Aerosol

from the Ozonolysis of α-Pinene. *Proc. Natl. Acad. Sci. U.S.A.* **2014**, *111*, 7552−7557.
(28) Berkemeier, T.; Shiraiwa, M.; Pöschl, U.; Koop, T. Competition between Water Uptake and Ice Nucleation by Glassy Organic Aerosol Particles. *Atmos. Chem. Phys. Discuss.* **2014**, *14*, 16451−16492.
(29) Adler, G.; Koop, T.; Haspel, C.; Taraniuk, I.; Moise, T.; Koren, I.; Heiblum, R. H.; Rudich, Y. Formation of Highly Porous Aerosol Particles by Atmospheric Freeze-Drying in Ice Clouds. *Proc. Natl. Acad. Sci. U.S.A.* **2013**, *110*, 20414−20419.
(30) You, Y.; Renbaum-Wolff, L.; Carreras-Sospedra, M.; Hanna, S. J.; Hiranuma, N.; Kamal, S.; Smith, M. L.; Zhang, X.; Weber, R. J.; Shilling, J. E.; et al. Images reveal that atmospheric particles can undergo liquid−liquid phase separations. *Proc. Natl. Acad. Sci. U.S.A.* **2012**, *109*, 13188−13193.
(31) O'Brien, R. E.; Neu, A.; Epstein, S. A.; MacMillan, A. C.; Wang, B.; Kelly, S. T.; Nizkorodov, S. A.; Laskin, A.; Moffet, R. C.; Gilles, M. K. Physical Properties of Ambient and Laboratory-Generated Secondary Organic Aerosol. *Geophys. Res. Lett.* **2014**, 2014GL060219.
(32) Lignell, H.; Hinks, M. L.; Nizkorodov, S. A. Exploring Matrix Effects on Photochemistry of Organic Aerosols. *Proc. Natl. Acad. Sci. U.S.A.* **2014**, *111*, 13780−13785.
(33) Saukko, E.; Lambe, A. T.; Massoli, P.; Koop, T.; Wright, J. P.; Croasdale, D. R.; Pedernera, D. A.; Onasch, T. B.; Laaksonen, A.; Davidovits, P.; et al. Humidity-dependent phase state of SOA particles from biogenic and anthropogenic precursors. *Atmos. Chem. Phys.* **2012**, *12*, 7517−7529.
(34) Shiraiwa, M.; Pöschl, U.; Knopf, D. A. Multiphase Chemical Kinetics of NO_3 Radicals Reacting with Organic Aerosol Components from Biomass Burning. *Environ. Sci. Technol.* **2012**, *46*, 6630−6636.
(35) Debenedetti, P. G.; Stillinger, F. H. Supercooled Liquids and the Glass Transition. *Nature* **2001**, *410*, 259−267.
(36) Zobrist, B.; Marcolli, C.; Pedernera, D. A.; Koop, T. Do Atmospheric Aerosols Form Glasses? *Atmos. Chem. Phys.* **2008**, *8*, 5221−5244.
(37) Zobrist, B.; Soonsin, V.; Luo, B. P.; Krieger, U. K.; Marcolli, C.; Peter, T.; Koop, T. Ultra-Slow Water Diffusion in Aqueous Sucrose Glasses. *Phys. Chem. Chem. Phys.* **2011**, *13*, 3514−3526.
(38) Mikhailov, E.; Vlasenko, S.; Martin, S. T.; Koop, T.; Pöschl, U. Amorphous and Crystalline Aerosol Particles Interacting with Water Vapor: Conceptual Framework and Experimental Evidence for Restructuring, Phase Transitions and Kinetic Limitations. *Atmos. Chem. Phys.* **2009**, *9*, 9491−9522.
(39) Tong, S. R.; Wu, L. Y.; Ge, M. F.; Wang, W. G.; Pu, Z. F. Heterogeneous Chemistry of Monocarboxylic Acids on α-Al_2O_3 at Different Relative Humidities. *Atmos. Chem. Phys.* **2010**, *10*, 7561−7574.
(40) Usher, C. R.; Michel, A. E.; Grassian, V. H. Reactions on Mineral Dust. *Chem. Rev.* **2003**, *103*, 4883−4939.
(41) Shilling, J. E.; Connelly, B. M.; Tolbert, M. A. Uptake of Small Oxygenated Organic Molecules onto Ammonium Nitrate under Upper Tropospheric Conditions. *J. Phys. Chem. A* **2006**, *110*, 6687−6695.
(42) Wu, L.-Y.; Tong, S.-R.; Zhou, L.; Wang, W.-G.; Ge, M.-F. Synergistic Effects between SO_2 and HCOOH on α-Fe_2O_3. *J. Phys. Chem. A* **2013**, *117*, 3972−3979.
(43) Laskin, A.; Moffet, R. C.; Gilles, M. K.; Fast, J. D.; Zaveri, R. A.; Wang, B. B.; Nigge, P.; Shutthanandan, J. Tropospheric Chemistry of Internally Mixed Sea Salt and Organic Particles: Surprising Reactivity of NaCl with Weak Organic Acids. *J. Geophys. Res.: Atmos.* **2012**, *117*, D15302.
(44) Wang, B.; Laskin, A. Reactions between Water-Soluble Organic Acids and Nitrates in Atmospheric Aerosols: Recycling of Nitric Acid and Formation of Organic Salts. *J. Geophys. Res.: Atmos.* **2014**, *119*, 3335−3351.
(45) Kerminen, V. M.; Teinila, K.; Hillamo, R.; Pakkanen, T. Substitution of Chloride in Sea-Salt Particles by Inorganic and Organic Anions. *J. Aerosol. Sci.* **1998**, *29*, 929−942.
(46) Ghorai, S.; Wang, B.; Tivanski, A.; Laskin, A. Hygroscopic Properties of Internally Mixed Particles Composed of Nacl and Water-Soluble Organic Acids. *Environ. Sci. Technol.* **2014**, *48*, 2234−2241.
(47) Ma, Q.; Ma, J.; Liu, C.; Lai, C.; He, H. Laboratory Study on the Hygroscopic Behavior of External and Internal C2−C4 Dicarboxylic Acid−NaCl Mixtures. *Environ. Sci. Technol.* **2013**, *47*, 10381−10388.
(48) Laskina, O.; Young, M. A.; Kleiber, P. D.; Grassian, V. H. Infrared Extinction Spectroscopy and Micro-Raman Spectroscopy of Select Components of Mineral Dust Mixed with Organic Compounds. *J. Geophys. Res.: Atmos.* **2013**, *118*, 6593−6606.
(49) Ervens, B.; Turpin, B. J.; Weber, R. J. Secondary Organic Aerosol Formation in Cloud Droplets and Aqueous Particles (aqSOA): A Review of Laboratory, Field and Model Studies. *Atmos. Chem. Phys.* **2011**, *11*, 11069−11102.
(50) Drozd, G.; Woo, J.; Häkkinen, S. A. K.; Nenes, A.; McNeill, V. F. Inorganic Salts Interact with Oxalic Acid in Submicron Particles to Form Material with Low Hygroscopicity and Volatility. *Atmos. Chem. Phys.* **2014**, *14*, 5205−5215.
(51) Beardsley, R.; Jang, M.; Ori, B.; Im, Y.; Delcomyn, C. A.; Witherspoon, N. Role of Sea Salt Aerosols in the Formation of Aromatic Secondary Organic Aerosol: Yields and Hygroscopic Properties. *Environ. Chem.* **2013**, *10*, 167−177.
(52) Bateman, A. P.; Nizkorodov, S. A.; Laskin, J.; Laskin, A. Time-Resolved Molecular Characterization of Limonene/Ozone Aerosol Using High-Resolution Electrospray Ionization Mass Spectrometry. *Phys. Chem. Chem. Phys.* **2009**, *11*, 7931−7942.
(53) Shilling, J. E.; Chen, Q.; King, S. M.; Rosenoern, T.; Kroll, J. H.; Worsnop, D. R.; McKinney, K. A.; Martin, S. T. Particle Mass Yield in Secondary Organic Aerosol Formed by the Dark Ozonolysis of α-Pinene. *Atmos. Chem. Phys.* **2008**, *8*, 2073−2088.
(54) Liu, S.; Shilling, J. E.; Song, C.; Hiranuma, N.; Zaveri, R. A.; Russell, L. M. Hydrolysis of Organonitrate Functional Groups in Aerosol Particles. *Aerosol. Sci. Technol.* **2012**, *46*, 1359−1369.
(55) Wang, B.; Knopf, D. A. Heterogeneous Ice Nucleation on Particles Composed of Humic-Like Substances Impacted by O_3. *J. Geophys. Res.: Atmos.* **2011**, *116*, D03205.
(56) Laskin, A.; Moffet, R. C.; Gilles, M. K.; Fast, J. D.; Zaveri, R. A.; Wang, B. B.; Nigge, P.; Shutthanandan, J. Tropospheric Chemistry of Internally Mixed Sea Salt and Organic Particles: Surprising Reactivity of NaCl with Weak Organic Acids. *J. Geophys. Res.: Atmos.* **2012**, *117*, D15302.
(57) Laskin, A., Electron Beam Analysis and Microscopy of Individual Particles. In *Fundamentals and Applications in Aerosol Spectroscopy*; Signorell, R., Reid, J., Eds.; Taylor and Francis Books, Inc.: Boca Raton, FL, 2010; pp 463−491.
(58) Laskin, A.; Cowin, J. P.; Iedema, M. J. Analysis of Individual Environmental Particles Using Modern Methods of Electron Microscopy and X-ray Microanalysis. *J. Electron Spectrosc. Relat. Phenom.* **2006**, *150*, 260−274.
(59) Liu, Y.; Yang, Z.; Desyaterik, Y.; Gassman, P. L.; Wang, H.; Laskin, A. Hygroscopic Behavior of Substrate-Deposited Particles Studied by Micro-FTIR Spectroscopy and Complementary Methods of Particle Analysis. *Anal. Chem.* **2008**, *80*, 633−642.
(60) Cain, J. P.; Gassman, P. L.; Wang, H.; Laskin, A. Micro-FTIR Study of Soot Chemical Composition-Evidence of Aliphatic Hydrocarbons on Nascent Soot Surfaces. *Phys. Chem. Chem. Phys.* **2010**, *12*, 5206−5218.
(61) Moffet, R. C.; Tivanski, A. V.; Gilles, M. K. Scanning X-ray Transmission Microscopy: Applications in Atmospheric Aerosol Research. In *Fundamentals and Applications in Aerosol Spectroscopy*; Signorell, R., Reid, J. P., Eds.; Taylor and Francis Books, Inc: Boca Raton, FL, 2010; pp 419−462.
(62) Moffet, R. C.; Henn, T.; Laskin, A.; Gilles, M. K. Automated Chemical Analysis of Internally Mixed Aerosol Particles Using X-ray Spectromicroscopy at the Carbon K-Edge. *Anal. Chem.* **2010**, *82*, 7906−7914.
(63) Moffet, R. C.; Rödel, T. C.; Kelly, S. T.; Yu, X. Y.; Carroll, G. T.; Fast, J.; Zaveri, R. A.; Laskin, A.; Gilles, M. K. Spectro-Microscopic Measurements of Carbonaceous Aerosol Aging in Central California. *Atmos. Chem. Phys.* **2013**, *13*, 10445−10459.
(64) Kelly, S. T.; Nigge, P.; Prakash, S.; Laskin, A.; Wang, B.; Tyliszczak, T.; Leone, S. R.; Gilles, M. K. An Environmental Sample

Chamber for Reliable Scanning Transmission X-ray Microscopy Measurements under Water Vapor. *Rev. Sci. Instrum.* **2013**, *84*, 073708.
(65) Roach, P. J.; Laskin, J.; Laskin, A. Molecular Characterization of Organic Aerosols Using Nanospray-Desorption/Electrospray Ionization-Mass Spectrometry. *Anal. Chem.* **2010**, *82*, 7979−7986.
(66) Roach, P. J.; Laskin, J.; Laskin, A. Nanospray Desorption Electrospray Ionization: An Ambient Method for Liquid-Extraction Surface Sampling in Mass Spectrometry. *Analyst* **2010**, *135*, 2233−2236.
(67) Roach, P. J.; Laskin, J.; Laskin, A. Higher-Order Mass Defect Analysis for Mass Spectra of Complex Organic Mixtures. *Anal. Chem.* **2011**, *83*, 4924−4929.
(68) Nizkorodov, S. A.; Laskin, J.; Laskin, A. Molecular Chemistry of Organic Aerosols through the Application of High Resolution Mass Spectrometry. *Phys. Chem. Chem. Phys.* **2011**, *13*, 3612−3629.
(69) You, Y.; Smith, M. L.; Song, M.; Martin, S. T.; Bertram, A. K. Liquid−Liquid Phase Separation in Atmospherically Relevant Particles Consisting of Organic Species and Inorganic Salts. *Int. Rev. Phys. Chem.* **2014**, *33*, 43−77.
(70) Riedler, M.; de Castro, A. R. B.; Kolmakov, A.; Löfken, J. O.; Nowak, C.; Soldatov, A. V.; Wark, A.; Yalovega, G.; Möller, T. Na 1*s* Photoabsorption of Free and Deposited NaCl Clusters: Development of Bond Length with Cluster Size. *Phys. Rev. B* **2001**, *64*, 245419.
(71) Dette, H. P.; Qi, M.; Schröder, D. C.; Godt, A.; Koop, T. Glass-Forming Properties of 3-Methylbutane-1,2,3-Tricarboxylic Acid and Its Mixtures with Water and Pinonic Acid. *J. Phys. Chem. A* **2014**, *118*, 7024−7033.
(72) Petters, M. D.; Wex, H.; Carrico, C. M.; Hallbauer, E.; Massling, A.; McMeeking, G. R.; Poulain, L.; Wu, Z.; Kreidenweis, S. M.; Stratmann, F. Towards Closing the Gap between Hygroscopic Growth and Activation for Secondary Organic Aerosol − Part 2: Theoretical Approaches. *Atmos. Chem. Phys.* **2009**, *9*, 3999−4009.
(73) Frosch, M.; Bilde, M.; DeCarlo, P. F.; Jurányi, Z.; Tritscher, T.; Dommen, J.; Donahue, N. M.; Gysel, M.; Weingartner, E.; Baltensperger, U. Relating Cloud Condensation Nuclei Activity and Oxidation Level of α-Pinene Secondary Organic Aerosols. *J. Geophys. Res.: Atmos.* **2011**, *116*, D22212.
(74) Koop, T.; Luo, B. P.; Tsias, A.; Peter, T. Water Activity as the Determinant for Homogeneous Ice Nucleation in Aqueous Solutions. *Nature* **2000**, *406*, 611−614.
(75) Williams, M. L.; Landel, R. F.; Ferry, J. D. The Temperature Dependence of Relaxation Mechanisms in Amorphous Polymers and Other Glass-Forming Liquids. *J. Am. Chem. Soc.* **1955**, *77*, 3701−3707.
(76) Schill, G. P.; Tolbert, M. A. Heterogeneous Ice Nucleation on Phase-Separated Organic-Sulfate Particles: Effect of Liquid vs. Glassy Coatings. *Atmos. Chem. Phys.* **2013**, *13*, 4681−4695.
(77) Power, R. M.; Simpson, S. H.; Reid, J. P.; Hudson, A. J. The Transition from Liquid to Solid-like Behaviour in Ultrahigh Viscosity Aerosol Particles. *Chem. Sci.* **2013**, *4*, 2597−2604.
(78) Bones, D. L.; Reid, J. P.; Lienhard, D. M.; Krieger, U. K. Comparing the Mechanism of Water Condensation and Evaporation in Glassy Aerosol. *Proc. Natl. Acad. Sci. U.S.A.* **2012**, *109*, 11613−11618.
(79) Price, H. C.; Murray, B. J.; Mattsson, J.; O'Sullivan, D.; Wilson, T. W.; Baustian, K. J.; Benning, L. G. Quantifying Water Diffusion in High-Viscosity and Glassy Aqueous Solutions Using a Raman Isotope Tracer Method. *Atmos. Chem. Phys.* **2014**, *14*, 3817−3830.
(80) Johnson, D.; Marston, G. The Gas-Phase Ozonolysis of Unsaturated Volatile Organic Compounds in the Troposphere. *Chem. Soc. Rev.* **2008**, *37*, 699−716.
(81) Yasmeen, F.; Vermeylen, R.; Szmigielski, R.; Iinuma, Y.; Böge, O.; Herrmann, H.; Maenhaut, W.; Claeys, M. Terpenylic Acid and Related Compounds: Precursors for Dimers in Secondary Organic Aerosol from the Ozonolysis of α- and β-Pinene. *Atmos. Chem. Phys.* **2010**, *10*, 9383−9392.
(82) Thornton, J. A.; Kercher, J. P.; Riedel, T. P.; Wagner, N. L.; Cozic, J.; Holloway, J. S.; Dubé, W. P.; Wolfe, G. M.; Quinn, P. K.; Middlebrook, A. M.; et al. A large atomic chlorine source inferred from mid-continental reactive nitrogen chemistry. *Nature* **2010**, *464*, 271−274.
(83) Wu, Z. J.; Nowak, A.; Poulain, L.; Herrmann, H.; Wiedensohler, A. Hygroscopic Behavior of Atmospherically Relevant Water-Soluble Carboxylic Salts and Their Influence on the Water Uptake of Ammonium Sulfate. *Atmos. Chem. Phys.* **2011**, *11*, 12617−12626.
(84) Knopf, D. A.; Alpert, P. A.; Wang, B.; O'Brien, R. E.; Kelly, S. T.; Laskin, A.; Gilles, M. K.; Moffet, R. C. Microspectroscopic Imaging and Characterization of Individually Identified Ice Nucleating Particles from a Case Field Study. *J. Geophys. Res.: Atmos.* **2014**, *119*, 10,365−10,381.